Theory of Electromagnons in CuO

Kun Cao,[1] Feliciano Giustino,[1] and Paolo G. Radaelli[2]
[1]Department of Materials, University of Oxford, Parks Road, Oxford OX1 3PH, United Kingdom
[2]Clarendon Laboratory, Department of Physics, University of Oxford, Parks Road, Oxford OX1 3PU, United Kingdom
(Received 25 November 2014; revised manuscript received 17 February 2015; published 11 May 2015)

We develop a theory of electromagnons in CuO by combining a symmetry analysis based on irreducible corepresentations, *ab initio* calculations, and simulations of spin dynamics using a model Hamiltonian and the Landau-Lifshitz-Gilbert equation. We show that the electromagnon measured in [Jones *et al.*, Nat. Commun. 5, 3787 (2014)] with the electric field along the [101] direction originates from a magnetoelectric coupling mediated by Dzyaloshinskii-Moriya interactions and consists of a rigid rotation of the Cu spins around the axis defined by the electric field. Furthermore we predict the existence of a second electromagnon originating from exchange striction and coupled to electric fields along the [010] direction in the AF2 phase.

DOI: 10.1103/PhysRevLett.114.197201 PACS numbers: 75.85.+t, 63.20.-e, 77.80.-e

Magnetoferrelectric materials have attracted considerable attention owing to their potential applications in novel multifunctional devices [1,2]. An attractive feature of magnetoferroelectrics is that optical phonons and spin waves can become coupled via magnetoelectric interactions, yielding a new elementary excitation called an electromagnon [3]. This new excitation may open new pathways for encoding and manipulating information using light-spin interactions in quantum materials. Intuitively, electromagnons can be understood as being magnons coupled with a macroscopic electric polarization, which in turn can respond to external electric fields. The polarization and the magnon are coupled either by the Dzyaloshinskii-Moriya (DM) interaction [4] or by the exchange striction (ES) mechanism [5,6].

During the past decade, electromagnons have been observed in several magnetoferroelectrics, in particular, $R\mathrm{MnO_3}$ [7,8] and $R\mathrm{Mn_2O_5}$ [9], where R is a rare earth element among Tb, Dy, Gd, Eu, and Y. In these systems the electromagnon is thought to originate from the ES mechanism. The electric polarization is associated with the variation of the scalar exchange field $\Delta(\mathbf{S}_i \cdot \mathbf{S}_j) \approx \mathbf{S}_i \cdot \Delta\mathbf{S}_j + \Delta\mathbf{S}_i \cdot \mathbf{S}_j$, where $\mathbf{S}_i$ represents the local magnetic moments and $\Delta\mathbf{S}_i$ their variation due to the electromagnon. At variance with the ES mechanism, for electromagnons to originate from the DM interaction, the electric polarization needs to be associated with the variation of the vector field $\Delta(\mathbf{S}_i \times \mathbf{S}_j) \approx \mathbf{S}_i \times \Delta\mathbf{S}_j + \Delta\mathbf{S}_i \times \mathbf{S}_j$. In the case of helical magnets, it was proposed that the DM mechanism can indeed couple magnons and electric fields perpendicular to the spin plane [4]. Subsequent measurements on $\mathrm{Eu_{0.5}Y_{0.45}MnO_3}$ supported this proposal [10].

Recently, CuO was found to be a high-temperature multiferroic with $T_N = 230$ K [11]. Below T_N, CuO exhibits multiferroicity in the so-called AF2 phase. This phase is characterized by an incommensurate spin spiral with modulation vector $\mathbf{q}_2 = (0.506, 0, -0.483)$ in reciprocal lattice coordinates, and a saturated electric polarization of 160 $\mu\mathrm{C/m^2}$ [11]. At temperatures below 213 K, CuO exhibits a collinear magnetic phase called AF1, characterized by the modulation vector $\mathbf{q}_1 = (0.5, 0, -0.5)$. Very recently, electromagnons with an excitation energy of $\sim$3 meV were observed in the AF2 phase of CuO for electric fields along the [101] crystallographic direction [12]. To the best of our knowledge, no detailed atomistic theory of such an electromagnon has been developed. In particular, the finding of Ref. [12] cannot be explained using the mechanism of Ref. [4] since the [101] direction is not perpendicular to the spin plane.

In this Letter we combine a symmetry analysis, *ab initio* calculations, and simulations of spin dynamics based on a model spin Hamiltonian in order to show that the electromagnon observed in CuO originates from the DM interaction. Additionally, our analysis indicates that it should be possible to excite an ES electromagnon in the AF2 phase by using an electric field along the [010] direction.

CuO crystallizes in a monoclinic lattice within the $C2/c$ space group. The primitive cell contains two Cu sublattices, one located at $y = b/4$ (I) and the other at $y = 3b/4$ (II), with b denoting the lattice parameter along [010], as shown in Fig. 1. In order to describe the AF2 phase, we follow Refs. [13,14] and approximate $\mathbf{q}_2$ by the commensurate wave vector $\tilde{\mathbf{q}}_2 = (0.5, 0, -0.5)$. In this structure the spins of sublattice I lie in the ac plane, while those of sublattice II are parallel to the b axis. Within each sublattice the spins are aligned ferromagnetically or antiferromagnetically along the [101] and $[10\bar{1}]$ directions, respectively. The complete spin structure can be seen in Fig. 2(a).

We start with a symmetry analysis to show that the recently observed electromagnon in CuO [12] cannot originate from an ES mechanism. A group-theoretical analysis of the magnetic structures of CuO was given in

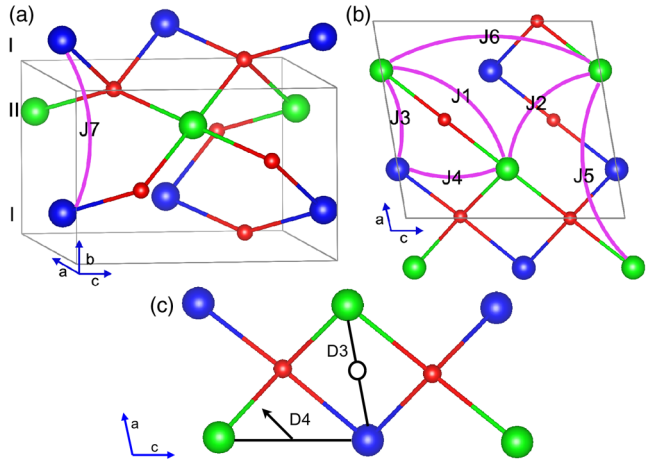

FIG. 1 (color online). Side view (a) and top view (b) of a ball-and-stick model of CuO. The red spheres indicate O atoms, while the blue and green spheres represent Cu atoms belonging to sublattice I and sublattice II, respectively. The sublattices are indicated in (a), and the unit cell boundaries are shown as gray lines. The purple connectors indicate the superexchange interactions summarized in Table IV of the Supplemental Material [15]. (c) The black lines indicate $\mathbf{D}_3$ and $\mathbf{D}_4$, the arrow indicates the direction of $\mathbf{D}_4$, and the open circle indicates one center of inversion.

Ref. [18] using the representations of the magnetic space group $C2/c1'$. Here we employ the alternative method introduced in Ref. [19], which is based on the irreducible corepresentations of the $C2/c$ space group. Our approach is simpler than that of Ref. [18] but equally rigorous. The Cu spins in the AF2 magnetic structure can be described by

$$\mathbf{S} = (\hat{\mathbf{u}}\Delta_1 + \hat{\mathbf{b}} i\Delta_2) e^{i\mathbf{q}_2\cdot\mathbf{R}} + \text{c.c.}, \tag{1}$$

where Δ_1 and Δ_2 are the two irreducible corepresentations of the space group $C2/c$ with a propagation vector

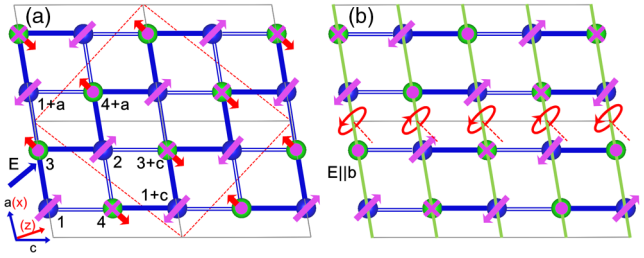

FIG. 2 (color online). Schematic illustrations of the AF2 magnetic structure of CuO within a $2 \times 1 \times 2$ supercell and of the magnetic response to an applied field. The purple arrows, crosses, and dots denote the orientation of the spins in the ground state. The red arrows indicate the direction of rotation of each spin, and the green lines highlight the spin chains. (a) Response to an electric field along [101]. The blue lines indicate the sign of $\Delta(\mathbf{S}_i \times \mathbf{S}_j)$, with a single (double) line for $+$ ($-$). (b) Response to an electric field along [010]. The blue lines indicate $\Delta(\mathbf{S}_i \cdot \mathbf{S}_j)$ with the same sign convention as in (a).

$\mathbf{q}_2$, $\hat{\mathbf{u}}$, $\hat{\mathbf{b}}$ are unit vectors parallel to the [101] and [010] directions, respectively, and $\mathbf{R}$ denotes a lattice vector. A comprehensive description of this formalism is given in the Supplemental Material [15]. For an ES magnon to couple with electromagnetic radiation, the exhange field $\Delta(\mathbf{S}_i \cdot \mathbf{S}_j)$ must correspond to a long wavelength excitation ($\mathbf{q} = 0$); that is, the magnon wave vector has to be $\pm\mathbf{q}_2$. In addition, an electromagnon is only present when $\Delta(\mathbf{S}_i \cdot \mathbf{S}_j)$ is nonzero, which only happens when the following conditions are fulfilled: $\Delta\mathbf{S}_i$ is perpendicular to $\mathbf{S}_i$, it is contained in the plane defined by $\hat{\mathbf{u}}$ and $\hat{\mathbf{b}}$, and the spins of the two sublattices rotate in opposite directions [15]. As a result, the variation of the spin pattern corresponding to an ES electromagnon can be described by

$$\Delta\mathbf{S} = (\hat{\mathbf{b}}\Delta_1 + \hat{\mathbf{u}} i\Delta_2) e^{-i\mathbf{q}_2\cdot\mathbf{R}} + \text{c.c.} \tag{2}$$

By combining Eqs. (1) and (2), we find that the exchange field $\mathbf{S}\cdot\Delta\mathbf{S}$ transforms as $\Delta_1 \otimes i\Delta_2^* = \Gamma_2$, where $\otimes$ indicates the tensor product of corepresentations (see the Supplemental Material [15] for representation and corepresentation tables and tensor products). Since the Γ_2 irreducible representation of the space group $C2/c$ preserves the twofold axis but not the c glide, an electric polarization is only allowed along the b axis. This reasoning shows that the exchange-striction mechanism cannot explain the observed electromagnon with electric field along [101]. If we repeat the same reasoning for a polarization along [010], we find that in this latter case an ES electromagnon is allowed by symmetry. We note that our choice of approximating the spin structure in the AF2 phase by a commensurate wave vector does not affect our symmetry analysis since $(0.5, 0, -0.5)$ is not a special point in the Brillouin zone.

At variance with the ES mechanism, a symmetry analysis along the same lines shows that the DM interaction can produce an exchange field $\Delta(\mathbf{S}_i \times \mathbf{S}_j)$ which transforms as Γ_4 [15]. Since the Γ_4 representation is compatible with an electric polarization in the ac plane, we deduce that a DM electromagnon is indeed allowed for electric fields along [101].

The above symmetry considerations indicate that a DM electromagnon is indeed allowed in CuO, although they do not provide information on the strength of the DM coupling, on the direction of the electromagnon polarization, and on the excitation energy. In order to obtain this information, we now move to *ab initio* calculations of the magnetic structure of CuO.

The magnetic properties of CuO can be described by the following spin Hamiltonian [13,14]:

$$\hat{H} = \sum_{ij} J_{ij}\mathbf{S}_i \cdot \mathbf{S}_j + \mathbf{D}_{ij} \cdot (\mathbf{S}_i \times \mathbf{S}_j) - \sum_i (\mathbf{K} \cdot \mathbf{S}_i)^2 + \hat{H}_{\text{me}}. \tag{3}$$

In this expression the first term describes superexchange interactions, as shown in Fig. 1. The second term describes the DM interaction, with the indices of the vectors $\mathbf{D}_{ij}$ carrying the same meaning as for the exchange couplings. The third term represents the single-ion anisotropy, and the last term stands for the magnetoelectric coupling. The interaction Hamiltonian $\hat{H}_{\mathrm{me}}$ responsible for electromagnons in the AF2 phase will be determined below. The exchange parameters J_1, J_2, and J_7 in Eq. (3) stabilize a collinear magnetic structure within each sublattice, while J_3 and J_4 are responsible for the intersublattice interactions, leading to frustration. The DM parameter $\mathbf{D}_3$ vanishes since it connects two Cu atoms related by inversion symmetry, as shown in Fig. 1(c) [20]. There is no symmetry restriction for $\mathbf{D}_4$; in our model, $\mathbf{D}_4$ makes the spins in the two Cu sublattices to be nearly perpendicular to each other. Our chosen direction of $\mathbf{D}_4$ is shown in Fig. 1(c). The anisotropy parameter $\mathbf{K}$ has the easy axis along b and applies to sublattice II only in order to stabilize the AF2 phase.

With reference to Eq. (3), the coupling between a macroscopic electric field and magnons in CuO is made possible by the intrinsic dependence of the coupling parameters J_{ij} and $\mathbf{D}_{ij}$ on the atomic positions, which in turn can be modulated by the coupling to an external field. In principle, this could be accounted for by expanding the coupling parameters to first order in the displacement, e.g., $J_{ij} = J^0_{ij} + (\partial J_{ij}/\partial u)(\partial u/\partial E)E$, where J^0_{ij} are for the equilibrium structure, u denotes a collective atomic displacement, and E the electric field. In practice, since this procedure is numerically intensive, we here proceed by directly applying an electric field and then calculating the corresponding change in the atomic positions and the spin structure.

In order to perform these calculations, we used density-functional theory in the generalized gradient approximation of Perdew, Burke, and Ernzerhof [21], including Hubbard corrections [22], as implemented in VASP [23,24]. The core-valence interaction was described by means of the projector augmented-wave method [25] and a plane waves basis set with a kinetic energy cutoff of 37 Ry was employed. The calculations were performed using a $2 \times 1 \times 2$ supercell at the experimental lattice parameters. The electric polarization was computed using the Berry phase method [26]. We optimized the atomic geometry and found that the AF2 phase is a local energy minimum. By fixing the Hund coupling constant to 1 eV and testing several Hubbard parameters, we found that $U = 4$ eV produces a static electric polarization of 150 $\mu\mathrm{C/m^2}$, in agreement with experiments. Accordingly, we only present results for this value of U. The atomic displacements induced by an applied electric field $\mathbf{E}$ were calculated as $\delta\tau_{I\alpha} = \sum_{J\beta} K^{-1}_{I\alpha,J\beta} Z^*_{J\beta} E_\beta$ [27–29], where K represents the matrix of force constants, Z^* the Born effective charges, the capital indices identify the atoms in the unit cell, and the Greek indices indicate Cartesian directions. The Born charges and the matrix of force constants were determined via density functional perturbation theory [30], and the displacements were obtained for an applied electric field of 10^9 V/m. This choice ensures that the system remains in the local energy minimum corresponding to the AF2 phase.

Given the experimental findings of Ref. [12] and the symmetry analysis presented above, we proceed by investigating the magnetic response induced by electric fields along the optical axes [101] and [010], respectively. Our calculations indicate that the details of the variations $\Delta\mathbf{S}$ are sensitive to the calculations parameters. On the contrary, we find that the variations of the scalar products $\Delta(\mathbf{S}_i \cdot \mathbf{S}_j)$ and of the vector products $\Delta(\mathbf{S}_i \times \mathbf{S}_j)$ are relatively insensitive to such details; hence, these can be used reliably for analyzing the magnetic response to the electric field. We find that electric fields along [101] and [010] induce the changes $\Delta(\mathbf{S}_i \times \mathbf{S}_j)$ and $\Delta(\mathbf{S}_i \cdot \mathbf{S}_j)$, respectively, with i and j belonging to different Cu sublattices. This observation is fully consistent with our symmetry analysis (above). In particular, the variations $\Delta(\mathbf{S}_i \times \mathbf{S}_j)$ corresponding to Cu atoms i and j in different sublattices exhibit nonvanishing components only along b, and alternating signs along directions both a and b. This result is illustrated schematically in Fig. 2(a).

In order to validate this pattern, we performed the reverse procedure: that is, we performed constrained spin-DFT calculations by enforcing these patterns and determined the corresponding polarization. In the case of the electric field along the [101] direction, we consider a configuration whereby the spins of sublattice II rotate around the axis defined by the spin direction of sublattice I, as shown in Fig. 2(a).

Figure 2 of the Supplemental Material [15] shows the calculated electric polarization as a function of the spin rotation angle θ. The calculated polarization is along [101], in line with the experimental observations, and varies with the angle as $\sin\theta$, in line with our expectations. If we instead repeat the calculations by neglecting spin-orbit interactions, the polarization is found to vanish. This is a clear indication that the coupling between spin and polarization along [101] in CuO finds its origin in the DM interaction.

We now consider a polarization along the [010] direction, as our symmetry analysis indicates that, in this case, we should expect an ES electromagnon. When we apply an electric field along [010], we obtain variations of the scalar products $\Delta(\mathbf{S}_i \cdot \mathbf{S}_j)$ exhibiting $C2$ symmetry, with ferromagnetic and antiferromagnetic signs alternating along the c axis. These variations can be realized by considering out-of-phase rigid rotations of the spin chains along the a direction within the spin plane, with a wave vector $\mathbf{q} = \mathbf{q}_2 + (0, 0, 1)$. This is shown schematically in Fig. 2(b). Using this pattern in a constrained spin-DFT calculation, we verified that the rotation of the spins induces an electric polarization along [010]. This finding indicates that, in this case, we are in the

presence of an ES electromagnon, consistent with our symmetry analysis.

Based on our constrained spin-DFT calculations, we propose the following interaction Hamiltonian for the coupling between external fields and electromagnons in CuO:

$$\begin{aligned}\hat{H}_{\mathrm{me}} = {} & E_u \alpha \sum_i [(\mathbf{S}_{4,i} - \mathbf{S}_{4,i+a}) \times (\mathbf{S}_{2,i} + \mathbf{S}_{2,i+b}) \\ & + (\mathbf{S}_{3,i} + \mathbf{S}_{3,i-b}) \times (\mathbf{S}_{1,i+a} - \mathbf{S}_{1,i})]_b \\ & + E_b \beta \sum_i [(\mathbf{S}_{4,i} + \mathbf{S}_{4,i-b}) \cdot (\mathbf{S}_{1,i} - \mathbf{S}_{1,i+c}) \\ & + (\mathbf{S}_{2,i} + \mathbf{S}_{2,i+b}) \cdot (\mathbf{S}_{3,i} - \mathbf{S}_{1,3+c})]. \end{aligned} \quad (4)$$

Here the subscripts u and b indicate the components along the unit vectors $\mathbf{u}$ and $\mathbf{b}$, that is, the [101] and the [010] direction, respectively; the subscripts in $\mathbf{S}_{n,i}$ indicate the Cu atom in a unit cell following the convention in Fig. 2 and the unit cell, respectively. This interaction Hamiltonian was obtained from the corresponding terms in Eq. (3) by setting the signs according to the spin patterns obtained here via constrained spin-DFT. The magnetoelectric coupling constants appearing in Eq. (4) are defined as $\alpha = \mathbf{u} \cdot \partial(\mathbf{D}_3 + \mathbf{D}_4)/\partial \mathbf{E}$ and $\beta = \mathbf{b} \cdot \partial J_4/\partial \mathbf{E}$, and the values obtained from our calculations are reported in Table IV of the Supplemental Material [15].

The two terms in Eq. (4) define the coupling of the magnetic structure of CuO to electric fields along [101] and [010], respectively. The first and second lines may give rise to DM electromagnons and ES electromagnons, respectively. In order to identify and characterize these excitations within a fully dynamical framework, we proceed by solving the Landau-Lifshitz-Gilbert equation based on the complete spin Hamiltonian given by Eqs. (3) and (4). We obtain [31,32]

$$\hbar \frac{d\mathbf{S}_i}{dt} = \mathbf{S}_i \times \frac{\partial \hat{H}}{\partial \mathbf{S}_i} + \hbar \alpha_{\mathrm{G}} \frac{\mathbf{S}_i}{|\mathbf{S}_i|} \times \frac{\partial \mathbf{S}_i}{\partial t}, \quad (5)$$

where t is the time, $\partial \hat{H}/\partial \mathbf{S}_i$ represents the effective magnetic field experienced by the spin $\mathbf{S}_i$, α_G is the Gilbert damping coefficent, and the norm of the spin is obtained from $|\mathbf{S}_i|^2 = \frac{1}{2}(\frac{1}{2}+1)$. Since the precise values of the parameters in the spin Hamiltonian $\hat{H}$ of CuO are still under debate [13,14,33,34], we simplify here the task of solving Eq. (5) by considering average semiempirical parameters from the literature [13,14,33,34]. The parameters adopted are reported in Table IV of the Supplemental Material [15], and the sensitivity of our results to this choice is discussed below. Using these parameters and Monte Carlo simulations we verified that the AF2 phase is indeed the ground state magnetic structure, and the transition temperature matches (by construction) the experimental $T_N = 230$ K. We solved Eq. (5) using the fourth-order Runge-Kutta method [31,32], by applying an electric field pulse at $t = 0$, and by following

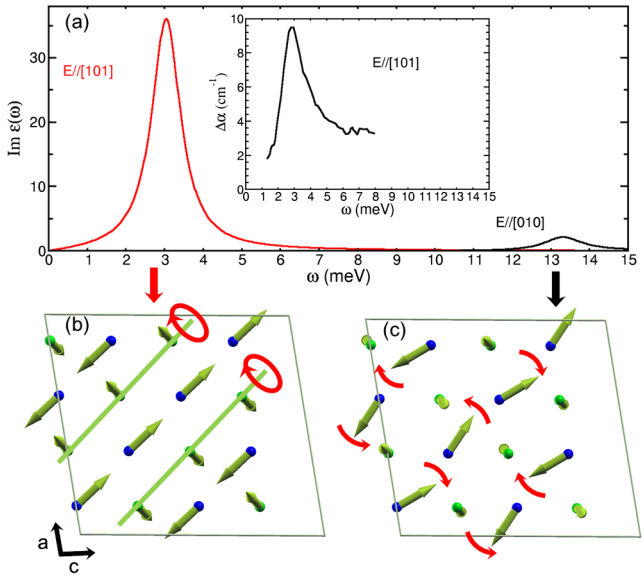

FIG. 3 (color online). (a) Electromagnon spectra calculated using Eq. (5) and electric fields along the [101] (red solid line) and the [010] (black solid line) direction, respectively. The inset shows the experimental electromagnon spectrum of CuO [12]. (b) and (c) Schematic illustrations of the oscillations of the Cu spins in each case.

the evolution of the polarization at subsequent times. The Fourier transform of the polarization can be used to extract the imaginary part of the dielectric function $\epsilon(\omega)$, from which electromagnon excitations can be identified. We repeated this operation twice, for the initial electric field oriented along the [101] and the [010] direction, respectively.

Figure 3(a) shows our calculated dielectric functions. In the case where the applied electric field is along [101], we can see a sharp resonance around 3 meV, which is consistent with the experimental data displayed in the inset of Fig. 3(a) [12]. The structure of the electromagnon corresponding to this resonance can be analyzed by following the real-time evolution of $\Delta \mathbf{S}_i$ after the pulse. We obtain a phason mode at $\mathbf{q}_2$ (or at the Γ point in the spin corotating frame), as shown schematically in Fig. 3(b). This finding is consistent with the $\Delta \mathbf{S}_i$'s determined by the direct approach and shown in Fig. 2.

In the case of an electric pulse along the [010] direction we observe a resonance at 13.5 meV [Fig. 3(a)]. This resonance corresponds to an electromagnon at $\mathbf{q} = \mathbf{q}_2 + (0, 0, 1)$, featuring an out-of-phase rotation of the spins along the [101] direction. This excitation is schematically illustrated in Fig. 3(c). The optical spectra reported in Ref. [12] were recorded in the range 0–8 meV; therefore, our present findings suggest that new experiments are needed in order to possibly observe a second, weaker resonance coresponding to an ES electromagnon at energies > 10 meV.

We tested the sensitivity of these results to the choice of parameters in the spin Hamiltonian, as shown in Fig. 4 of

the Supplemental Material [15]. Since our parameters are able to reproduce the measured Néel temperature, our current estimate for the energy of the ES electromagnon should be realistic.

Recently, a Heisenberg model with higher-order bilinear-biquadratic coupling has been proposed for reproducing the magnetic phase diagram of CuO without including DM interactions [35]. Our present theory of the high-energy electromagnon (which arises from ES) can naturally be extended to the model of Ref. [35]. However, the low-energy electromagnon is not captured by the higher-order coupling terms of that model since they yield a vanishing magnetoelectric coupling at first order. This reinforces the need for including DM interactions in the study of electromagnons in CuO.

In summary, by combining a symmetry analysis based on irreducible corepresentations, *ab initio* calculations, and time-domain simulations of the magnetoelectric response of CuO, we showed that the electromagnon measured in Ref. [12] is of DM origin and corresponds to a phason mode. In addition, our study indicates that it should be possible to observe a second electromagnon in CuO, originating from the ES mechanism. We hope that the present investigation will motivate further experiments to search for the high-energy electromagnon predicted here. More generally, the present work sets a blueprint for future studies of new elementary excitations in complex magnetic materials.

The authors are grateful to S. P. P. Jones and J. Lloyd-Hughes for the fruitful discussions. This work was funded by EPSRC Grant No. EP/J003557/1, entitled "New Concepts in Multiferroics and Magnetoelectrics." Calculations were performed at the Oxford Supercomputing Centre and at the Oxford Materials Modelling Laboratory.

[1] S.-W. Cheong and M. Mostovoy, Nat. Mater. **6**, 13 (2007).
[2] M. Fiebig, J. Phys. D **38**, R123 (2005).
[3] G. Smolenskii and I. Chupis, Sov. Phys. Usp. **25**, 475 (1982).
[4] H. Katsura, A. V. Balatsky, and N. Nagaosa, Phys. Rev. Lett. **98**, 027203 (2007).
[5] R. Valdés Aguilar, M. Mostovoy, A. B. Sushkov, C. L. Zhang, Y. J. Choi, S.-W. Cheong, and H. D. Drew, Phys. Rev. Lett. **102**, 047203 (2009).
[6] A. B. Sushkov, M. Mostovoy, R. V. Aguilar, S.-W. Cheong, and H. D. Drew, J. Phys. Condens. Matter **20**, 434210 (2008).
[7] A. Pimenov, A. A. Mukhin, V. Ivanov, V. Travkin, A. Balbashov, and A. Loidl, Nat. Phys. **2**, 97 (2006).
[8] R. Valdés Aguilar, A. B. Sushkov, C. L. Zhang, Y. J. Choi, S.-W. Cheong, and H. D. Drew, Phys. Rev. B **76**, 060404 (2007).
[9] A. B. Sushkov, R. V. Aguilar, S. Park, S.-W. Cheong, and H. D. Drew, Phys. Rev. Lett. **98**, 027202 (2007).
[10] Y. Takahashi, R. Shimano, Y. Kaneko, H. Murakawa, and Y. Tokura, Nat. Phys. **8**, 121 (2012).
[11] T. Kimura, Y. Sekio, H. Nakamura, T. Siegrist, and A. P. Ramirez, Nat. Mater. **7**, 291 (2008).
[12] S. P. P. Jones, S. M. Gaw, K. I. Doig, D. Prabhakaran, E. Hétroy Wheeler, A. T. Boothroyd, and J. Lloyd-Hughes, Nat. Commun. **5**, 3787 (2014).
[13] G. Giovannetti, S. Kumar, A. Stroppa, J. van den Brink, S. Picozzi, and J. Lorenzana, Phys. Rev. Lett. **106**, 026401 (2011).
[14] G. Jin, K. Cao, G.-C. Guo, and L. He, Phys. Rev. Lett. **108**, 187205 (2012).
[15] See Supplemental Material at http://link.aps.org/supplemental/10.1103/PhysRevLett.114.197201, which includes Refs. [16,17], for details of the symmetry analysis and spin dynamics simulations.
[16] C. Bradley and A. Cracknell, *The Mathematical Theory of Symmetry in Solids* (Clarendon Press, Oxford, 1972).
[17] O. Kovalev, *Representations of the Crystallographyc Space Groups—Irreducible Representations, Induced Representations and Corepresentations* (Gordon and Breach, Yverdon, Switzerland, 1993).
[18] P. Tolédano, N. Leo, D. D. Khalyavin, L. C. Chapon, T. Hoffmann, D. Meier, and M. Fiebig, Phys. Rev. Lett. **106**, 257601 (2011).
[19] P. G. Radaelli and L. C. Chapon, Phys. Rev. B **76**, 054428 (2007).
[20] T. Moriya, Phys. Rev. **120**, 91 (1960).
[21] J. P. Perdew, K. Burke, and M. Ernzerhof, Phys. Rev. Lett. **77**, 3865 (1996).
[22] A. I. Liechtenstein, V. I. Anisimov, and J. Zaanen, Phys. Rev. B **52**, R5467 (1995).
[23] G. Kresse and J. Hafner, Phys. Rev. B **47**, 558 (1993).
[24] G. Kresse and J. Furthmuller, Phys. Rev. B **54**, 11169 (1996).
[25] P. E. Blochl, Phys. Rev. B **50**, 17953 (1994).
[26] R. D. King-Smith and D. Vanderbilt, Phys. Rev. B **47**, 1651 (1993).
[27] J. Íñiguez, Phys. Rev. Lett. **101**, 117201 (2008).
[28] A. Malashevich, S. Coh, I. Souza, and D. Vanderbilt, Phys. Rev. B **86**, 094430 (2012).
[29] A. Scaramucci, E. Bousquet, M. Fechner, M. Mostovoy, and N. A. Spaldin, Phys. Rev. Lett. **109**, 197203 (2012).
[30] S. Baroni, S. de Gironcoli, A. Dal Corso, and P. Giannozzi, Rev. Mod. Phys. **73**, 515 (2001).
[31] M. Mochizuki, N. Furukawa, and N. Nagaosa, Phys. Rev. Lett. **104**, 177206 (2010).
[32] K. Cao, G.-C. Guo, and L. He, J. Phys. Condens. Matter **24**, 206001 (2012).
[33] A. Filippetti and V. Fiorentini, Phys. Rev. Lett. **95**, 086405 (2005).
[34] X. Rocquefelte, M.-H. Whangbo, A. Villesuzanne, S. Jobic, F. Tran, K. Schwarz, and P. Blaha, J. Phys. Condens. Matter **22**, 045502 (2010).
[35] K. Pasrija and S. Kumar, Phys. Rev. B **88**, 144418 (2013).